Available online at www.sciencedirect.com
SCIENCE DIRECT®
International Journal of Heat and Mass Transfer 49 (2006) 219–229
International Journal of HEAT and MASS TRANSFER
www.elsevier.com/locate/ijhmt

Meshless method for radiation heat transfer in graded index medium

L.H. Liu *

School of Energy Science and Engineering, Harbin Institute of Technology, 92 West Dazhi Street, Harbin 150001, People's Republic of China

Received 29 March 2005; received in revised form 1 July 2005
Available online 5 October 2005

Abstract

Because ray goes along a curved path determined by the Fermat principle, curved ray tracing is very difficult and complex in graded index media. To avoid the difficult and complex computation of curved ray trajectories, a meshless local Petrov–Galerkin approach based on discrete-ordinate equations is developed to solve the radiative transfer problem in multi-dimensional absorbing–emitting–scattering semitransparent graded index media. A moving least square approximation is used to construct the shape function. Two particular test problems in radiative transfer are taken as examples to verify this meshless approach. The predicted temperature distributions and the dimensionless radiative heat fluxes are determined by the proposed method and compared with the other benchmark approximate solutions. The results show that the meshless local Petrov–Galerkin approach based on discrete-ordinate equations has a good accuracy in solving the radiative transfer problems in absorbing–emitting–scattering semitransparent graded index media.

Keywords: Radiative heat transfer; Graded index; Semitransparent medium; Meshless method

1. Introduction

Due to the structural characteristics of material or a possible temperature dependency, the refractive index of a medium may be a function of the spatial position. In this case, rays propagating inside the medium are not straight lines, but curved lines determined by the Fermat principle [1,2]. The radiative heat transfer in a semitransparent medium with variable spatial refractive index (or graded index) is of great interest in thermo-optical systems, and has evoked the wide interest of many researchers. Recently, many ray-tracing techniques have been presented by Ben Abdallah et al. [3–6], Huang et al. [7,8], Liu et al. [9,10] to solve the radiative transfer problem in the semitransparent medium with graded refractive index. Because the ray goes along a curved path determined by the Fermat principle, the curved ray tracing is very difficult and complex in the graded index medium. At present, the methods based on the curved ray-tracing techniques were mainly limited to one-dimensional radiative transfer problems. The numerical approaches of the radiative transfer equation in multi-dimensional semitransparent graded index media require considerable effort.

* Tel.: +86 451 8640 2237; fax: +86 451 8622 1048.
E-mail address: lhliu@hit.edu.cn

0017-9310/$ - see front matter © 2005 Elsevier Ltd. All rights reserved.
doi:10.1016/j.ijheatmasstransfer.2005.07.013

Nomenclature

a	coefficients for MLS approximation in Eq. (18)
$\mathbf{a}$	vector of coefficient a
$\mathbf{A}$	matrix defined in Eq. (21)
$\mathbf{B}$	matrix defined in Eq. (22)
g	quartic spline function with compact support
$\mathbf{i},\mathbf{j},\mathbf{k}$	unit vectors into the x-, y- and z-directions, respectively
I	radiative intensity
I_b	blackbody radiative intensity
K	coefficients in linear equations
L	slab thickness, side length of rectangular medium
N_{MLS}	number of the nodes used for MLS approximation
N_{node}	total node number scattered in the entire domain and its boundary
N_θ	number of polar angular discretization
N_φ	number of azimuthal angular discretization
N_ξ	number of the discretization in direction cosine ξ
n	refractive index
$\mathbf{n}_w$	unit outward normal vector of the boundary wall
$\mathbf{p}$	monomial basis
q	radiative heat flux
$\mathbf{r}$	vector of spatial position
s	abscissas on the ray trajectory
$\mathbf{s}_1$	vector defined in Eq. (2b), $\mathbf{s}_1 = -\mathbf{i}\sin\varphi + \mathbf{j}\cos\varphi$
T	temperature
T_{wi}	temperature of wall i
u	trial function
$\mathbf{u}$	vector of trial function
v	test function
V_S	local sub-domain for weighted integration
$V_\mathbf{x}$	domain of definition of MLS approximation for the trial function at $\mathbf{x}$
$w^{m,n}$	weight corresponding to the direction (m,n)
w^{MLS}	MLS weight function
x,y,z	Cartesian coordinates
$\mathbf{x}$	spatial position vector of point, $\mathbf{x} = [x,y,z]^T$
$\mathbf{x}_Q$	Gaussian quadrature point
α	partial derivative of refractive index respect to x, $\alpha = \frac{1}{n}\frac{\partial n}{\partial x}$
α_{MLS}, α_{GQ}	dimensionless size parameters
β	partial derivative of refractive index respect to y, $\beta = \frac{1}{n}\frac{\partial n}{\partial y}$
γ	partial derivative of refractive index respect to z, $\gamma = \frac{1}{n}\frac{\partial n}{\partial z}$
η	direction cosine, $\eta = \sin\theta\sin\varphi$
δ_{ij}	Kronecker's delta
ε	wall emissivity
θ	polar angle
$\Delta\theta$	polar angle step
κ_a	absorption coefficient
κ_s	scattering coefficient
μ	direction cosine, $\mu = \sin\theta\cos\varphi$
ξ	direction cosine, $\xi = \cos\theta$
σ	Stefan–Boltzmann constant
τ_L	optical thickness, $\tau_L = (\kappa_a + \kappa_s)L$
φ	azimuthal angle
$\Delta\varphi$	azimuthal angle step
Φ	scattering phase function
χ_θ,χ_φ	coefficients of the discretization equation, defined in Eqs. (9) and (14)
Ψ	dimensionless radiative heat flux
ω	single scattering albedo, $\omega = \kappa_s/(\kappa_a + \kappa_s)$
Ω	solid angle
$\mathbf{\Omega}$	vector of radiation direction, $\mathbf{\Omega} = \mathbf{i}\mu + \mathbf{j}\eta + \mathbf{k}\xi$
∇	spatial divergence operator, $\nabla = \mathbf{i}\frac{\partial}{\partial x} + \mathbf{j}\frac{\partial}{\partial y} + \mathbf{k}\frac{\partial}{\partial z}$

Subscripts

0	value at $z = 0$
av	averaged value
L	value at $z = L$
w	value at wall boundary

Superscripts

$m,n,m',n',m\pm1/2,n\pm1/2$,	angular direction of radiation

To avoid the difficult and complex computation of curved ray trajectories, the methods, which are not based on curved ray-tracing, need to be developed for the solution of radiative heat transfer in graded index media. Among the methods which are not based on ray-tracing, the finite volume method (FVM), the discrete ordinates method (DOM), and the finite element method (FEM) are today probably the most popular methods to solve the radiative heat transfer in the medium with a uniform refractive index. However, because of the curved ray trajectory, these methods can not be directly used to solve the radiative transfer within the graded index medium. The streaming operator d/ds along a curved ray trajectory in original radiative trans-

fer equation for graded index media needs to be transformed into the form of spatial divergence operator, namely, $\mathbf{\Omega}\cdot\nabla I$. Following this way, Lemonnier and Dez [11] presented a DOM for the solution of radiative transfer across a one-dimensional slab with variable refractive index. Recently, Liu [12] deduced the three-dimensional radiative transfer equation within graded index media in Cartesian coordinate system and developed a FVM to solve the multi-dimensional radiative transfer in a graded index media. However, because the problem domain needs to be discretized into meshes, these traditional methods, especially the FEM, suffer from drawbacks such as tedious meshing and re-meshing.

In the community of computational mechanics, many meshless methods have been proposed for the problem of computational mechanics to avoid the tedious meshing and re-meshing. Meshless method is used to establish a system of algebraic equations for whole problem domain without the use of a predefined mesh. Meshless method use a set of nodes scattered within the problem domain and its boundaries. These scattered nodes do not form a mesh, which means that no information on the relationship between the nodes is required. Various methods belonging to this family are the element free Galerkin method, the meshless local Petrov–Galerkin (MLPG) method, the point interpolation method, the smoothed particle hydrodynamics method and so on [13–15]. Among these methods, MLPG method is a truly meshless method, which was originated by Atluri and Zhu [16] for the problem of computational mechanics. To the best knowledge of the author, meshless methods have not been used for the radiative transfer problem in graded index media.

In this paper, to avoid the difficult and complex computation of curved ray trajectories, a meshless local Petrov–Galerkin approach based on discrete-ordinate equations is developed to solve the radiative transfer problem in multi-dimensional absorbing–emitting–scattering semitransparent graded index media. A moving least square approximation is used to construct the shape function. Two particular test problems of radiative transfer inside the semitransparent graded index medium are taken as examples to verify this meshless approach.

2. Mathematical formulation

2.1. Discrete ordinate equation for graded index media

In the Cartesian coordinates system as shown in Fig. 1, the conservative form of radiative transfer equation within graded index medium can be written in the divergence form as [12]

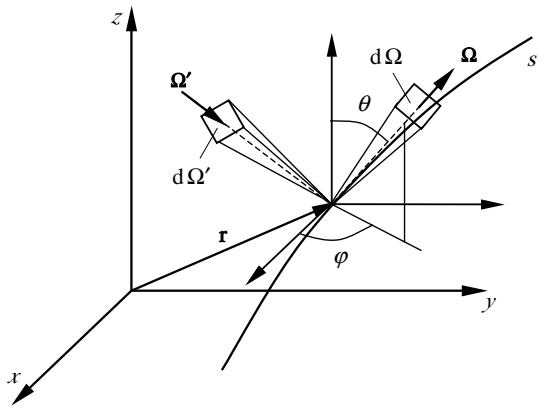

Fig. 1. Cartesian coordinate system.

$$\begin{aligned}&\mathbf{\Omega}\cdot\nabla I(\mathbf{r},\Omega)+\frac{1}{2n^2\sin\theta}\frac{\partial}{\partial\theta}\left\{\left[I(\mathbf{r},\Omega)(\xi\mathbf{\Omega}-\mathbf{k})\cdot\nabla n^2\right]\right\}\\&\quad+\frac{1}{2n^2\sin\theta}\frac{\partial}{\partial\varphi}\left\{I(\mathbf{r},\Omega)[\mathbf{s}_1\cdot\nabla n^2]\right\}+(\kappa_a+\kappa_s)I(\mathbf{r},\Omega)\\&\quad=n^2\kappa_a I_b+\frac{\kappa_s}{4\pi}\int_{4\pi}I(\mathbf{r},\Omega')\Phi(\Omega,\Omega')\,\mathrm{d}\Omega',\end{aligned}\tag{1}$$

where

$$\begin{aligned}\mathbf{\Omega}&=\mathbf{i}\mu+\mathbf{j}\eta+\mathbf{k}\xi\\&=\mathbf{i}\sin\theta\cos\varphi+\mathbf{j}\sin\theta\sin\varphi+\mathbf{k}\cos\theta,\end{aligned}\tag{2a}$$

$$\mathbf{s}_1=-\mathbf{i}\sin\varphi+\mathbf{j}\cos\varphi.\tag{2b}$$

Here, $\mathbf{i}$, $\mathbf{j}$, and $\mathbf{k}$ are unit vectors into x-, y- and z-directions, respectively. The radiative transfer equation in graded index medium is different from that in uniform index medium. Terms involving a partial derivative with respect to an angular coordinate in Eq. (1) are referred as angular redistribution terms, which specially account for the curvature of the optical path in the graded index medium. For a opaque diffuse boundary wall, the boundary condition of Eq. (1) is given as follows:

$$\begin{aligned}I(\mathbf{r}_w,\Omega)=\varepsilon_w n_w^2\frac{\sigma T_w^4}{\pi}+\frac{(1-\varepsilon_w)}{\pi}\\\times\int_{\mathbf{n}_w\cdot\mathbf{\Omega}'\geqslant 0}I(\mathbf{r}_w,\Omega')(\mathbf{n}_w\cdot\mathbf{\Omega}')\,\mathrm{d}\Omega',\quad\mathbf{n}_w\cdot\mathbf{\Omega}<0,\end{aligned}\tag{3}$$

where $\mathbf{n}_w$ is the unit outward normal vector of the boundary wall.

In the DOM, Eq. (1) is solved for a set of different directions, and the integrals over direction are replaced by numerical quadratures. Considering that Eq. (1) contains two angular redistribution terms, we employ the piecewise constant angular (PCA) quadrature. In the PCA quadrature, the total solid angle is divided uniform in the polar θ and azimuthal φ directions. The numbers

of divisions are denoted by N_θ and N_φ. From this we can write Eq. (1) in discrete ordinates form as

$$\begin{aligned}&\boldsymbol{\Omega}^{m,n}\cdot\nabla I(\mathbf{r},\Omega^{m,n})\\&\quad+\frac{1}{2n^2\sin\theta^m}\left[\frac{\partial}{\partial\theta}\left\{\left[I(\mathbf{r},\Omega)(\xi\boldsymbol{\Omega}-\mathbf{k})\cdot\nabla n^2\right]\right\}\right]_{\Omega=\Omega^{m,n}}\\&\quad+\frac{1}{2n^2\sin\theta^m}\left[\frac{\partial}{\partial\varphi}\left\{I(\mathbf{r},\Omega)\left[\mathbf{s}_1\cdot\nabla n^2\right]\right\}\right]_{\Omega=\Omega^{m,n}}\\&\quad+(\kappa_a+\kappa_s)I(\mathbf{r},\Omega^{m,n})\\&\quad=n^2\kappa_a I_b+\frac{\kappa_s}{4\pi}\sum_{m'=1}^{N_\theta}\sum_{n'=1}^{N_\varphi}I(\mathbf{r},\Omega^{m',n'})\Phi(\Omega^{m',n'},\Omega^{m,n})w_\theta^{m'}w_\varphi^{n'}.\end{aligned}\tag{4}$$

Here, the discrete polar and azimuthal angles are expressed as follows:

$$\theta^m=(m-1/2)\Delta\theta,\quad m=1,2,\ldots,N_\theta,\tag{5a}$$

$$\varphi^n=(n-1/2)\Delta\varphi,\quad n=1,2,\ldots,N_\varphi,\tag{5b}$$

where $\Delta\theta=\pi/N_\theta$ and $\Delta\varphi=2\pi/N_\varphi$. For each discrete ordinate, the corresponding weight is obtained as

$$w_\theta^m=\int_{\theta^{m-1/2}}^{\theta^{m+1/2}}\sin\theta\,\mathrm{d}\theta=\cos\theta^{m-1/2}-\cos\theta^{m+1/2},\tag{6a}$$

$$w_\varphi^n=\int_{\varphi^{n-1/2}}^{\varphi^{n+1/2}}\mathrm{d}\varphi=\varphi^{n+1/2}-\varphi^{n-1/2},\tag{6b}$$

where

$$\theta^{m+1/2}=(\theta^m+\theta^{m+1})/2,\tag{7a}$$

$$\varphi^{n+1/2}=(\varphi^n+\varphi^{n+1})/2.\tag{7b}$$

Since Eq. (4) contains two angular redistribution terms, the derivatives with respect to polar θ and azimuthal φ angles must be approximated by finite differences. Similar to the treatment of angular redistribution terms of the DOM in the spherical or cylindrical medium with a uniform refractive index [17], we may approximately write the first angular redistribution term as

$$\begin{aligned}&\frac{1}{2n^2\sin\theta^m}\left[\frac{\partial}{\partial\theta}\left\{\left[I(\xi\boldsymbol{\Omega}-\mathbf{k})\cdot\nabla n^2\right]\right\}\right]_{\Omega=\Omega^{m,n}}\\&\quad\simeq\frac{\chi_\theta^{m+1/2,n}I^{m+1/2,n}-\chi_\theta^{m-1/2,n}I^{m-1/2,n}}{w_\theta^m}.\end{aligned}\tag{8}$$

The values of $\chi_\theta^{m\pm1/2,n}$ depend only on the differencing scheme and, therefore, are independent of intensity and may be determined by examining a particularly simple intensity field. For example, if the medium is isothermal, then $I=n^2I_b=$ constant. This then leads to

$$\begin{aligned}&\chi_\theta^{m+1/2,n}-\chi_\theta^{m-1/2,n}\\&\quad=\frac{w_\theta^m}{2n^2\sin\theta^m}\left[\frac{\partial}{\partial\theta}\left[(\xi\boldsymbol{\Omega}-\mathbf{k})\cdot\nabla n^2\right]\right]_{\Omega=\Omega^{m,n}}\\&\quad=\frac{w_\theta^m}{2n^2\sin\theta^m}[\cos2\theta^m(\alpha\cos\varphi^n+\beta\sin\varphi^n)-\gamma\sin2\theta^m],\end{aligned}\tag{9}$$

where the refractive index derivatives, α, β, and γ, are defined respectively as

$$\alpha=\frac{1}{n}\frac{\partial n}{\partial x}=\frac{1}{2n^2}\frac{\partial n^2}{\partial x},\tag{10a}$$

$$\beta=\frac{1}{n}\frac{\partial n}{\partial y}=\frac{1}{2n^2}\frac{\partial n^2}{\partial y},\tag{10b}$$

$$\gamma=\frac{1}{n}\frac{\partial n}{\partial z}=\frac{1}{2n^2}\frac{\partial n^2}{\partial z}.\tag{10c}$$

Eq. (9) may be used as a recursion formula for $\chi_\theta^{m+1/2,n}$, if a value for $\chi_\theta^{1/2,n}$ can be determined. This value can be found by comparing the following relations:

$$\begin{aligned}&\int_0^\pi\frac{1}{2n^2\sin\theta}\left[\frac{\partial}{\partial\theta}\left\{\left[I(\xi\boldsymbol{\Omega}-\mathbf{k})\cdot\nabla n^2\right]\right\}\right]\sin\theta\,\mathrm{d}\theta\\&\quad=\frac{1}{2n^2}[I(\xi\boldsymbol{\Omega}-\mathbf{k})\cdot\nabla n^2]_{\theta=\pi}-\frac{1}{2n^2}[I(\xi\boldsymbol{\Omega}-\mathbf{k})\cdot\nabla n^2]_{\theta=0}=0,\end{aligned}\tag{11a}$$

$$\begin{aligned}&\int_0^\pi\frac{1}{2n^2\sin\theta}\left[\frac{\partial}{\partial\theta}\left\{\left[I(\xi\boldsymbol{\Omega}-\mathbf{k})\cdot\nabla n^2\right]\right\}\right]\sin\theta\,\mathrm{d}\theta\\&\quad=\sum_{m=1}^{N_\theta}w_\theta^m\left[\frac{1}{2n^2\sin\theta}\frac{\partial}{\partial\theta}\{[I(\xi\boldsymbol{\Omega}-\mathbf{k})\cdot\nabla n^2]\}\right]_{\theta=\theta^m}\\&\quad=\sum_{m=1}^{N_\theta}\left[\chi_\theta^{m+1/2,n}I^{m+1/2,n}-\chi_\theta^{m-1/2,n}I^{m-1/2,n}\right]\\&\quad=\chi_\theta^{N_\theta+1/2,n}I^{N_\theta+1/2,n}-\chi_\theta^{1/2,n}I^{1/2,n},\end{aligned}\tag{11b}$$

Therefore,

$$\chi_\theta^{1/2,n}=\chi_\theta^{N_\theta+1/2,n}=0.\tag{12}$$

Similarly, the second angular redistribution term in Eq. (4) can be approximately written as

$$\begin{aligned}&\frac{1}{2n^2\sin\theta^m}\left[\frac{\partial}{\partial\varphi}\left\{I\left[\mathbf{s}_1\cdot\nabla n^2\right]\right\}\right]_{\Omega=\Omega^{m,n}}\\&\quad\simeq\frac{\chi_\varphi^{m,n+1/2}I^{m,n+1/2}-\chi_\varphi^{m,n-1/2}I^{m,n-1/2}}{w_\varphi^n}\end{aligned}\tag{13}$$

and the recursion formula for $\chi_\varphi^{m,n+1/2}$ is given as follows:

$$\begin{aligned}\chi_\varphi^{m,n+1/2}-\chi_\varphi^{m,n-1/2}&=\frac{w_\varphi^n}{2n^2\sin\theta^m}\left[\frac{\partial\mathbf{s}_1}{\partial\varphi}\cdot\nabla n^2\right]_{\Omega=\Omega^{m,n}}\\&=-\frac{w_\varphi^n}{\sin\theta^m}(\alpha\cos\varphi^n+\beta\sin\varphi^n),\end{aligned}\tag{14a}$$

$$\chi_\varphi^{m,1/2}=\chi_\varphi^{m,N_\varphi+1/2}=\frac{1}{2n^2\sin\theta^m}(\mathbf{j}\cdot\nabla n^2)=\frac{\beta}{\sin\theta^m}.\tag{14b}$$

Then the discrete ordinates equation can be rewritten as

$$\begin{aligned}&\boldsymbol{\Omega}^{m,n}\cdot\nabla I(\mathbf{r},\Omega^{m,n})\\&\quad+\frac{\chi_\theta^{m+1/2,n}I^{m+1/2,n}-\chi_\theta^{m-1/2,n}I^{m-1/2,n}}{w_\theta^m}\\&\quad+\frac{\chi_\varphi^{m,n+1/2}I^{m,n+1/2}-\chi_\varphi^{m,n-1/2}I^{m,n-1/2}}{w_\varphi^n}+(\kappa_a+\kappa_s)I^{m,n}\\&\quad=n^2\kappa_aI_b+\frac{\kappa_s}{4\pi}\sum_{m'=1}^{N_\theta}\sum_{n'=1}^{N_\varphi}I^{m',n'}\Phi^{m',n';m,n}w_\theta^{m'}w_\varphi^{n'}.\end{aligned}\tag{15}$$

Here, superscripts m, n, m', n', $m \pm 1/2$ and $n \pm 1/2$ denote the radiation directions.

To close Eq. (15), relations are needed between the intensities $I^{m\pm1/2,n\pm1/2}$ and $I^{m\pm1,n\pm1}$. One appropriate closure relation is based on the step scheme. Those are

$$\chi_\theta^{m+1/2,n} I^{m+1/2,n} = \max(\chi_\theta^{m+1/2,n},0) I^{m,n} - \max(-\chi_\theta^{m+1/2,n},0) I^{m+1,n}, \tag{16a}$$

$$\chi_\theta^{m-1/2,n} I^{m-1/2,n} = \max(\chi_\theta^{m-1/2,n},0) I^{m-1,n} - \max(-\chi_\theta^{m-1/2,n},0) I^{m,n}, \tag{16b}$$

$$\chi_\varphi^{m,n+1/2} I^{m,n+1/2} = \max(\chi_\varphi^{m,n+1/2},0) I^{m,n} - \max(-\chi_\varphi^{m,n+1/2},0) I^{m,n+1}, \tag{16c}$$

$$\chi_\varphi^{m,n-1/2} I^{m,n-1/2} = \max(\chi_\varphi^{m,n-1/2},0) I^{m,n-1} - \max(-\chi_\varphi^{m,n-1/2},0) I^{m,n}. \tag{16d}$$

By using the closure relations given in Eq. (16) and the linearization technique [18] of source term, the final discrete ordinate equation of radiative transfer in a three-dimensional graded index medium becomes

$$\begin{aligned}
&\boldsymbol{\Omega}^{m,n}\cdot\nabla I(\mathbf{r},\Omega^{m,n}) + \left[\frac{1}{w_\theta^m}\max\left(\chi_\theta^{m+1/2,n},0\right)\right.\\
&+\frac{1}{w_\theta^m}\max\left(-\chi_\theta^{m-1/2,n},0\right)+\frac{1}{w_\varphi^n}\max\left(\chi_\varphi^{m,n+1/2},0\right)\\
&+\frac{1}{w_\varphi^n}\max\left(-\chi_\varphi^{m,n-1/2},0\right)+(\kappa_a+\kappa_s)\\
&\left.-\frac{\kappa_s}{4\pi}\Phi^{m,n;m,n}w_\theta^m w_\varphi^n\right] I^{m,n}\\
&=\frac{1}{w_\theta^m}\max\left(-\chi_\theta^{m+1/2,n},0\right)I^{m+1,n}\\
&\quad+\frac{1}{w_\theta^m}\max\left(\chi_\theta^{m-1/2,n},0\right)I^{m-1,n}\\
&\quad+\frac{1}{w_\varphi^n}\max\left(-\chi_\varphi^{m,n+1/2},0\right)I^{m,n+1}\\
&\quad+\frac{1}{w_\varphi^n}\max\left(\chi_\varphi^{m,n-1/2},0\right)I^{m,n-1}+n^2\kappa_a I_b\\
&\quad+\frac{\kappa_s}{4\pi}\sum_{m',n';m\neq m',n\neq n'} I^{m',n'}\Phi^{m',n';m,n}w_\theta^{m'}w_\varphi^{n'}.
\end{aligned}\tag{17}$$

2.2. Moving least square approximation

In MLPG implementation, moving least square (MLS) approximation [13–16] is employed for constructing shape functions. Consider a spatial subdomain $V_{\mathbf{x}}$, the neighborhood of a point $\mathbf{x}$ and denoted as the domain of definition of MLS approximation for the trial function at $\mathbf{x}$, which is located within the problem domain. To approximate the distribution of a generic function u in $V_{\mathbf{x}}$, over a number of local nodes $\{\mathbf{x}_i\}$, $i = 1,2,\ldots,n$, the MLS approximant $\tilde{u}(\mathbf{x})$ of u, $\forall \mathbf{x} \in V_{\mathbf{x}}$, can be defined by

$$\tilde{u} = \sum_{j=0}^{k} p_j(\mathbf{x}) a_j(\mathbf{x}) = \mathbf{p}^{\mathrm{T}}(\mathbf{x})\mathbf{a}(\mathbf{x}), \tag{18}$$

where $\mathbf{p}^{\mathrm{T}}(\mathbf{x}) = [p_1(\mathbf{x}), p_2(\mathbf{x}), \ldots, p_k(\mathbf{x})]$ is a complete monomial basis of order k, and $\mathbf{a}(\mathbf{x})$ is a vector containing coefficients $a_j(\mathbf{x})$, $j = 1,2,\ldots,k$, which are functions of the spatial coordinates $\mathbf{x} = [x,y,z]^{\mathrm{T}}$. The coefficient vector $\mathbf{a}(\mathbf{x})$ is determined by minimizing a weighted discrete L_2 norm, defined as

$$J[\mathbf{a}(\mathbf{x})] = \sum_{i=1}^{N_{\mathrm{MLS}}} w_i^{\mathrm{MLS}}[\mathbf{p}^{\mathrm{T}}(\mathbf{x}_i)\mathbf{a}(\mathbf{x}) - \hat{u}_i]^2, \tag{19}$$

where $\mathbf{x}_i$ denotes the value of $\mathbf{x}$ at node i; $w_i^{\mathrm{MLS}}(\mathbf{x})$ is the MLS weight function associated with the node i, with $w_i^{\mathrm{MLS}}(\mathbf{x}) > 0$ for all $\mathbf{x}$ in the support of $w_i^{\mathrm{MLS}}(\mathbf{x})$; and N_{MLS} is the number of nodes in $V_{\mathbf{x}}$ for which the weight functions $w_i^{\mathrm{MLS}}(\mathbf{x}) > 0$. Here, $\hat{u}_i$ in Eq. (19) is the fictitious nodal value, and not the nodal value of unknown trial function $\tilde{u}_i$ in general.

The stationary of J with respect to $\mathbf{a}(\mathbf{x})$ leads to the following linear relation between $\mathbf{a}(\mathbf{x})$ and $\hat{\mathbf{u}}$.

$$\mathbf{A}(\mathbf{x})\mathbf{a}(\mathbf{x}) = \mathbf{B}(\mathbf{x})\hat{\mathbf{u}}, \tag{20}$$

where the matrices $\mathbf{A}(\mathbf{x})$, $\mathbf{B}(\mathbf{x})$ and $\hat{\mathbf{u}}$ are defined by

$$\mathbf{A}(\mathbf{x}) = \sum_{i=1}^{N_{\mathrm{MLS}}} w_i^{\mathrm{MLS}}(\mathbf{x})\mathbf{p}(\mathbf{x}_i)\mathbf{p}^{\mathrm{T}}(\mathbf{x}_i), \tag{21}$$

$$\mathbf{B}(\mathbf{x}) = \left[w_1^{\mathrm{MLS}}(\mathbf{x})\mathbf{p}(\mathbf{x}_1), w_2^{\mathrm{MLS}}(\mathbf{x})\mathbf{p}(\mathbf{x}_2), \ldots, w_{N_{\mathrm{MLS}}}^{\mathrm{MLS}}(\mathbf{x})\mathbf{p}(\mathbf{x}_{N_{\mathrm{MLS}}})\right], \tag{22}$$

$$\hat{\mathbf{u}} = \left[\hat{u}_1, \hat{u}_2, \ldots, \hat{u}_{N_{\mathrm{MLS}}}\right]. \tag{23}$$

Solving for $\mathbf{a}(\mathbf{x})$ from Eq. (20) and substituting it into Eq. (18) gives a relation which may be written in the form of an interpolation function similar to that used in finite element method, as

$$\tilde{u}(\mathbf{x}) = \sum_{i=1}^{N_{\mathrm{MLS}}} \phi_i(\mathbf{x})\hat{u}_i, \quad \forall \mathbf{x} \in V_{\mathbf{x}}, \tag{24}$$

where

$$\phi_i(\mathbf{x}) = \sum_{j=1}^{k} p_j(\mathbf{x})[\mathbf{A}^{-1}(\mathbf{x})\mathbf{B}(\mathbf{x})]_{ji}. \tag{25}$$

Here, $\phi_i(\mathbf{x})$ is usually called as the shape function of MLS approximation corresponding to nodal point $\mathbf{x}_i$.

The partial derivatives of the shape function are obtained as

$$\phi_{i,l}(\mathbf{x}) = \sum_{j=1}^{k} \left\{ p_{j,l}[\mathbf{A}^{-1}\mathbf{B}]_{ji} + p_j[\mathbf{A}^{-1}\mathbf{B}_{,l} + (\mathbf{A}^{-1})_{,l}\mathbf{B}]_{ji} \right\}, \tag{26}$$

where $(\ )_{,l} = \partial(\ )/\partial l$ represents the derivative with respect to spatial coordinate l, $l = x, y, z$.

2.3. Discretization and numerical implementation

Eq. (17) is weighted over the local sub-domain V_S, which is located entirely inside the global problem domain. The local sub-domain V_S can be taken to be a sphere or cube (for three-dimensional problem) centered at a point $\mathbf{x}_i$ in question. The integrated residuals are set to zero

$$\begin{aligned}
&\int_{V_S} \left\{ \mathbf{\Omega}^{m,n} \cdot \nabla I(\mathbf{r}, \Omega^{m,n}) + \left[\frac{1}{w_\theta^m} \max\left(\chi_\theta^{m+1/2,n}, 0\right) \right.\right. \\
&+ \frac{1}{w_\theta^m} \max\left(-\chi_\theta^{m-1/2,n}, 0\right) + \frac{1}{w_\varphi^n} \max\left(\chi_\varphi^{m,n+1/2}, 0\right) \\
&+ \frac{1}{w_\varphi^n} \max\left(-\chi_\varphi^{m,n-1/2}, 0\right) + (\kappa_a + \kappa_s) \\
&\left.\left. - \frac{\kappa_s}{4\pi} \Phi^{m,n;m,n} w_\theta^m w_\varphi^n \right] I^{m,n} \right\} v(\mathbf{x} - \mathbf{x}_i)\, \mathrm{d}V \\
&= \int_{V_S} \left[\frac{1}{w_\theta^m} \max\left(-\chi_\theta^{m+1/2,n}, 0\right) I^{m+1,n} \right. \\
&+ \frac{1}{w_\theta^m} \max\left(\chi_\theta^{m-1/2,n}, 0\right) I^{m-1,n} \\
&+ \frac{1}{w_\varphi^n} \max\left(-\chi_\varphi^{m,n+1/2}, 0\right) I^{m,n+1} \\
&+ \frac{1}{w_\varphi^n} \max\left(\chi_\varphi^{m,n-1/2}, 0\right) I^{m,n-1} + n^2 \kappa_a I_b \\
&\left. + \frac{\kappa_s}{4\pi} \sum_{m',n';m\neq m',n\neq n'} I^{m',n'} \Phi^{m',n';m,n} w_\theta^{m'} w_\varphi^{n'} \right] v(\mathbf{x} - \mathbf{x}_i)\, \mathrm{d}V, \\
&m = 1, 2, \ldots, N_\theta, \quad n = 1, 2, \ldots, N_\varphi, \quad i = 1, 2, \ldots, N_{\text{node}}.
\end{aligned} \tag{27}$$

where v is the test function, and N_{node} is the total number of nodes. Setting $u = I^{m,n}$, substitution of Eqs. (24)–(26) into Eq. (27) for all nodes leads to the following discretized system of linear equations:

$$\begin{aligned}
&\sum_{j=1}^{N_{\text{node}}} K_{ij}^{m,n} I_j^{m,n} = f_i^{m,n}, \quad m = 1, 2, \ldots, N_\theta, \\
&n = 1, 2, \ldots, N_\varphi, \quad i = 1, 2, \ldots, N_{\text{node}},
\end{aligned} \tag{28}$$

where

$$\begin{aligned}
K_{ij}^{m,n} = \int_{V_S} \left\{ \mathbf{\Omega}^{m,n} \cdot \nabla \phi_j(\mathbf{x}) + \left[\frac{1}{w_\theta^m} \max\left(\chi_\theta^{m+1/2,n}, 0\right) \right.\right. \\
+ \frac{1}{w_\theta^m} \max\left(-\chi_\theta^{m-1/2,n}, 0\right) \\
+ \frac{1}{w_\varphi^n} \max\left(\chi_\varphi^{m,n+1/2}, 0\right) \\
+ \frac{1}{w_\varphi^n} \max\left(-\chi_\varphi^{m,n-1/2}, 0\right) \\
\left.\left. + (\kappa_a + \kappa_s) - \frac{\kappa_s}{4\pi} \Phi^{m,n;m,n} w_\theta^m w_\varphi^n \right] \phi_j(\mathbf{x}) \right\} v(\mathbf{x} - \mathbf{x}_i)\, \mathrm{d}V,
\end{aligned} \tag{29a}$$

$$\begin{aligned}
f_i^{m,n} = \int_{V_S} \left[\frac{1}{w_\theta^m} \max\left(-\chi_\theta^{m+1/2,n}, 0\right) I^{m+1,n} \right. \\
+ \frac{1}{w_\theta^m} \max\left(\chi_\theta^{m-1/2,n}, 0\right) I^{m-1,n} \\
+ \frac{1}{w_\varphi^n} \max\left(-\chi_\varphi^{m,n+1/2}, 0\right) I^{m,n+1} \\
+ \frac{1}{w_\varphi^n} \max(\chi_\varphi^{m,n-1/2}, 0) I^{m,n-1} + n^2 \kappa_a I_b \\
\left. + \frac{\kappa_s}{4\pi} \sum_{m',n';m\neq m',n\neq n'} I^{m',n'} \Phi^{m',n';m,n} w_\theta^{m'} w_\varphi^{n'} \right] v(\mathbf{x} - \mathbf{x}_i)\, \mathrm{d}V.
\end{aligned} \tag{29b}$$

Eq. (28) is solved independently for each direction, and the boundary conditions (Eq. (3)) must be imposed on the inflow boundary. For each node i on the inflow boundary, the radiative intensity $I_i^{m,n}$ is given by the boundary condition, which can be directly imposed as follows:

$$K_{ij}^{m,n} = \delta_{ij}, \tag{30a}$$

$$f_i^{m,n} = I_i^{m,n}, \tag{30b}$$

where δ_{ij} is the Kronecker' delta.

Because the in-scattering term in the discrete-ordinates equation at the direction (m,n) contains the radiative intensities of the other directions, the global iterations similar to those used in the DOM are necessary to include the source and boundary conditions. For each discrete direction, the implementation of the MLPG method can be carried out according to the following routine:

Step 1: Choose a finite number of nodes in the problem domain and its boundaries; decide the basis function, MLS weight function and test function such that the MLS approximation is well defined and the weighted integration of radiative transfer equation can be implemented.

Step 2: Determine the local sub-domain V_S and its boundary for each node, and calculate Gaussian quadrature points $\mathbf{x}_Q$ in V_S.

Step 3: Determine the nodes $\mathbf{x}_i$ located in the domain of definition of the MLS approximation for the trial function at point $\mathbf{x}_Q$, i.e., those nodes with $w_i^{MLS}(\mathbf{x}_Q) > 0$.

Step 4: For those nodes in the domain of definition of the MLS approximation of trial function at point $\mathbf{x}_Q$; calculate shape function $\phi_i(\mathbf{x}_Q)$ and the derivatives $\phi_{i,x}(\mathbf{x}_Q)$, $\phi_{i,y}(\mathbf{x}_Q)$ and $\phi_{i,z}(\mathbf{x}_Q)$.

Step 5: Evaluate numerical integrals in Eqs. (29a) and (29b), and assemble contributions to the linear system Eq. (28) for all nodes.

Step 6: Solve the linear system for the fictitious nodal values $\widehat{I}^{m,n}$.

3. Results and discussions

Based on the theoretical and numerical analyses carried out above, a computer code has been developed, which is capable of modeling the multi-dimensional radiative transfer problem in graded index media. Node densification studies were also performed for the physical model to ensure that the essential physics are independent of node number. To verify the MLPG approach based on discrete-ordinate equations presented above for the radiative transfer problems in graded index media, two test problems are examined. The particular test cases are selected because exact, or at least very precise, solutions of the radiative heat transfer exist for comparison with the MLPG approach. For the following numerical study, a Gaussian quadrature with 6 integration points in each coordinate is employed to evaluate numerical integrals in Eq. (29). The quartic function [13] with compact supports is used to construct the weight function for the MLS approximation and the test function in the weighted integration of the dimensionless energy equation and the dimensionless radiative transfer equation

$$g(r) = \begin{cases} 1 - 6r^2 + 8r^3 - 3r^4, & r \leqslant 1 \\ 0, & r > 1 \end{cases}. \tag{31}$$

3.1. Radiative equilibrium in a one-dimensional graded index slab

As shown in Fig. 2, we consider a problem of radiative equilibrium in a one-dimensional semitransparent gray absorbing–emitting slab with thickness L. The boundaries are opaque, diffuse and gray walls. The emissivities of boundary walls are ε_0 and ε_L, and the temperatures of boundary walls are imposed as $T_0 = 1000$ K and $T_L = 1500$ K, respectively. The absorption coefficient κ_a is uniform over the slab, but the refractive index n of medium varies with the axis coordinate z. The boundary conditions are given by

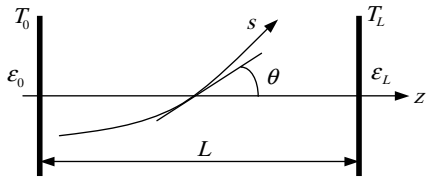

Fig. 2. Physical geometry of slab.

$$I(0,\xi) = \varepsilon_0 n_0^2 \frac{\sigma T_0^4}{\pi} + 2(1-\varepsilon_0)\int_{-1}^{0} I(0,\xi')\xi' \,\mathrm{d}\xi', \quad \xi \geqslant 0, \tag{32a}$$

$$I(L,\xi) = \varepsilon_L n_L^2 \frac{\sigma T_L^4}{\pi} + 2(1-\varepsilon_L)\int_{0}^{1} I(L,\xi')\xi' \,\mathrm{d}\xi', \quad \xi \leqslant 0, \tag{32b}$$

where n_0 and n_L are the refractive indices at boundaries of $z = 0$ and $z = L$, respectively. At radiative equilibrium, the temperature distribution within the medium is determined by [12]

$$T(z) = \left[\frac{\pi}{2\sigma n^2(z)} \sum_{m=1}^{N_\xi} I(z,\xi^m)\Delta\xi\right]^{0.25}. \tag{33}$$

The MLPG approach is applied to this one-dimensional radiative transfer problem. Linear and sinusoidal refractive indices are considered. 101 nodes are uniformly distributed in the problem domain $z \in [0, L]$ and its boundaries. The angular region $\xi = \cos\theta \in [-1, 1]$ is uniformly divided into $N_\xi = 40$ parts. The monomial basis $\mathbf{p}^T(\mathbf{x}) = [1, z, z^2]$ is used, and the weight function for the MLS approximation and the test function in the weighted integration of the discrete ordinate equation are given as follows:

$$w^{MLS}(z - z_i) = g\left(\left|\frac{z - z_i}{\alpha_{MLS}\Delta z}\right|\right), \tag{34}$$

$$v(z - z_i) = g\left(\left|\frac{z - z_i}{\alpha_{GQ}\Delta z}\right|\right), \tag{35}$$

where Δz is the average nodal spacing between two neighbor nodes, and the dimensionless size parameters $\alpha_{MLS} = 2.5$ and $\alpha_{GQ} = 1.5$ are used.

The temperature distributions within the slab are shown in Fig. 3 for three values of slab optical thickness, namely $\tau_L = 0.01$, $\tau_L = 1.0$ and $\tau_L = 3.0$, in the case of $n(z) = 1.2 + 0.6z/L$, $\varepsilon_0 = \varepsilon_L = 1$. This case was also used as a test case by Huang et al. [8] using the pseudo source adding method. As shown in Fig. 3, the MLPG results are in good agreement with the results obtained by using the pseudo source adding method. The maximum relative error based on the data in Ref. [8] is less than 1%. The effects of number of node number and angular discretization are shown in Fig. 4 for the case of $n(z) = 1.2 + 0.6z/L$, $\tau_L = 3$ and $\varepsilon_0 = \varepsilon_L = 1$. The comparison is quite good, even with a node number and

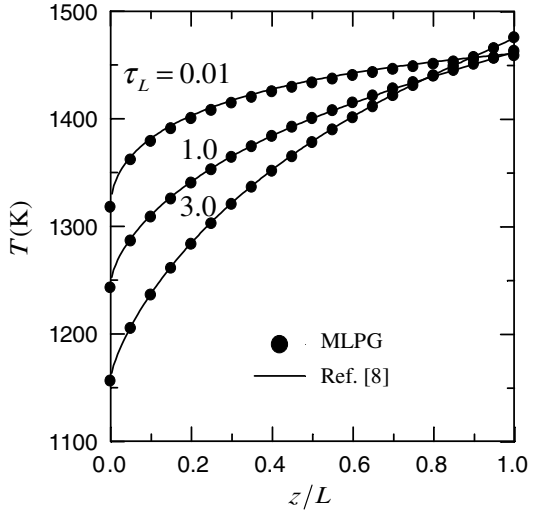

Fig. 3. Temperature distributions within slab for the case of $n(z) = 1.2 + 0.6z/L$, $\varepsilon_0 = \varepsilon_L = 1$.

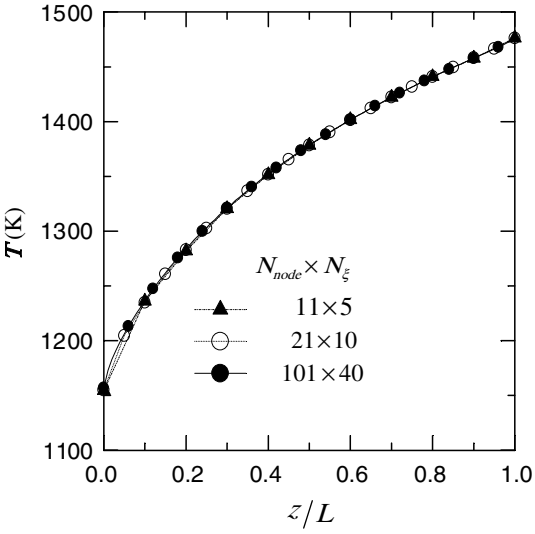

Fig. 4. Effects of number of node number and angular discretizations in the case of $n(z) = 1.2 + 0.6z/L$, $\tau_L = 3$ and $\varepsilon_0 = \varepsilon_L = 1$.

angular discretization only $N_{\text{node}} \times N_{\xi} = 11 \times 5$. The convergence of the MLPG approach is demonstrated in this figure. The time required for computation is less than 5 min on a personal computer with Intel Pentium Pro 450 MHz processor.

A nonlinear refractive index is also studied by using MLPG approach. The refractive index of medium within the slab varies sinusoidaly with the axis coordinate as $n(z) = 1.8 - 0.6\sin(\pi z/L)$. The slab optical thickness is $\tau_L = 1.0$. Fig. 5 shows the temperature distributions within the slab for two different conditions of wall emissivity, namely $\varepsilon_0 = \varepsilon_L = 1$ and $\varepsilon_0 = \varepsilon_L = 0.7$. As shown in Fig. 5, the MPLG results are in good agreement with the results obtained by Tan et al. [19] using the pseudo source adding method. The maximum relative error based on the data in Ref. [19] is less than 1%.

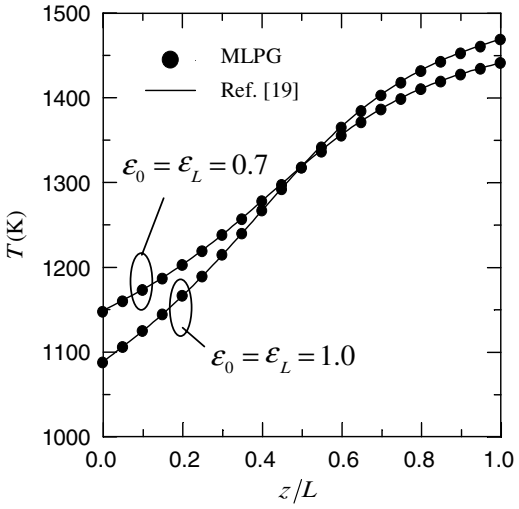

Fig. 5. Temperature distributions within slab for the case of $n(z) = 1.8 - 0.6\sin(\pi z/L)$, $\tau_L = 1$.

The MLPG approximation of the dimensionless radiative heat fluxes based on different nodes within the slab are profiled in Fig. 6 in the case of $n(z) = 1.2 + 0.6z/L$ and $\varepsilon_0 = \varepsilon_L = 1$. The dimensionless radiative heat flux is defined as

$$\Psi = 2\pi \int_{-1}^{1} I\mu \,\mathrm{d}\mu / n_0^2 \sigma (T_0^4 - T_L^4). \tag{36}$$

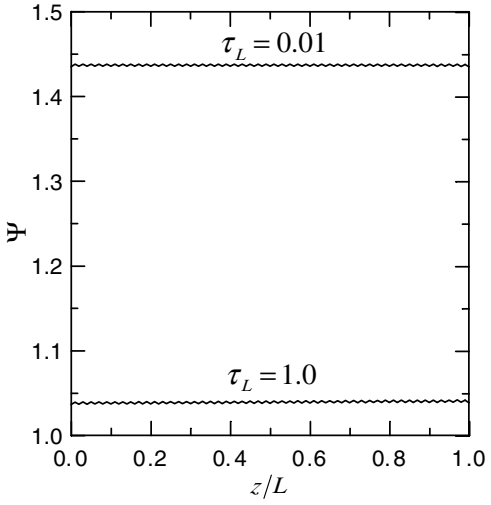

Fig. 6. MLPG approximation of the dimensionless radiative heat fluxes based on different nodes in the case of $n(z) = 1.2 + 0.6z/L$ and $\varepsilon_0 = \varepsilon_L = 1$.

Table 1
Dimensionless radiative heat flues in the case of blackbody boundaries and linear refractive index

n_0	n_L	τ_L	Ψ		
			RT [11]	DOM [11]	MLPG
1.0	1.5	0.1	0.9696	0.9696	0.9704
1.0	1.5	1	0.7243	0.7244	0.7241
1.0	1.5	10	0.1727	0.1729	0.1744
1.0	3.0	0.1	0.9872	0.9875	0.9947
1.0	3.0	1	0.8720	0.8719	0.8781
1.0	3.0	10	0.3152	0.3159	0.3256
1.0	5.0	0.1	0.9931	0.9929	1.0146
1.0	5.0	1	0.9250	0.9258	0.9461
1.0	5.0	10	0.4536	0.4563	0.4827

Theoretically, the exact dimensionless radiative heat fluxes based on different nodes are constant in this case, but the computed values of dimensionless radiative heat flux by using MLPG approach vary with the location of nodes and oscillate around its averaged value. This is very similar to FEM. However, the oscillation of dimensionless radiative heat flux computed by using MLPG approach is very small. The averaged dimensionless radiative heat fluxes for the cases of $\tau_L = 0.01$ and $\tau_L = 1.0$ are $\Psi_{\text{av}} = 1.437$ and $\Psi_{\text{av}} = 1.040$, respectively, and the maximum deviation of the dimensionless radiative heat flux, $|\Psi - \Psi_{\text{av}}|/\Psi_{\text{av}}$, is less than 0.3%.

The averaged dimensionless radiative heat fluxes in the case of blackbody boundary and linear refractive index are computed by using MLPG approach and given in Table 1. The results are compared with those obtained by Lemonnier et al. [11] using the curved ray-tracing technique (RT) and the DOM. From Table 1, it can be seen that the MLPG approach presented in this paper has a good accuracy in solving the dimensionless radiative heat fluxes in one-dimensional non-scattering graded index media. The maximum relative error of the dimensionless radiative heat flux based on the data obtained using the RT in Ref. [11] is less than 6.5%.

3.2. Isotropically scattering in a gray enclosure

As shown in Fig. 7, we consider the radiative heat transfer in a two-dimensional rectangular gray semi-transparent graded index medium enclosed by opaque boundaries with emissivity ε_{w}. The optical thickness based on the side length L ($L = 0.1$ m) of rectangular enclosure is $\tau_L = (\kappa_{\text{a}} + \kappa_{\text{s}})L = 0.1$. The lower wall is kept hot, but all other walls and the media enclosed by the rectangular enclosure are kept cold, The absorption coefficient κ_{a} and the scattering coefficient κ_{s} of the media enclosed by the rectangular enclosure is uniform, but the refractive index is a linear function of spatial position

$$n(x, y) = 1 + 2(x + y)/L. \tag{37}$$

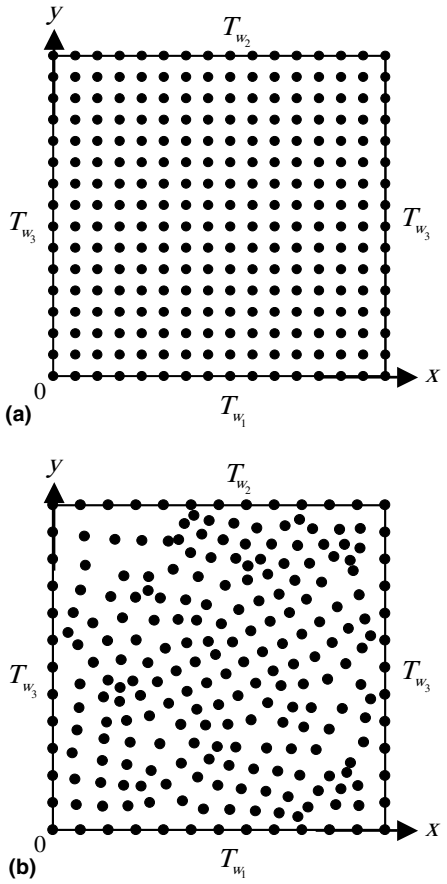

Fig. 7. Two-dimensional rectangular geometry and two patterns of nodal arrangement: (a) 225 nodes with regular arrangement and (b) 229 nodes with irregular arrangement.

The MLPG approach is applied to solve the radiative transfer problems in this rectangular enclosure. The monomial basis $\mathbf{p}^{\text{T}}(\mathbf{x}) = [1, x, y, x^2, xy, y^2]$ is used, and the weight function for the MLS approximation and the test function in the weighted integration of the discrete ordinate equation are given as follows:

$$w^{\text{MLS}}(\mathbf{x} - \mathbf{x}_i) = g\left(\left|\frac{x - x_i}{\alpha_{\text{MLS}}\Delta x}\right|\right) g\left(\left|\frac{y - y_i}{\alpha_{\text{MLS}}\Delta y}\right|\right), \tag{38}$$

$$v(\mathbf{x} - \mathbf{x}_i) = g\left(\left|\frac{x - x_i}{\alpha_{\text{GQ}}\Delta x}\right|\right) g\left(\left|\frac{y - y_i}{\alpha_{\text{GQ}}\Delta y}\right|\right), \tag{39}$$

where Δx and Δy are the average nodal spacing between two neighbor nodes in x and y coordinate directions, respectively, and the dimensionless size parameters $\alpha_{\text{MLS}} = 2.5$ and $\alpha_{\text{GQ}} = 1.5$ are used. The 4π solid angular region is uniformly divided into $N_\theta \times N_\varphi = 9 \times 18$ parts. Two patterns of nodal arrangement shown in Fig. 7 are considered: (a) 225 nodes with regular arrangement, and (b) 229 nodes with irregular arrangement. The dimensionless net radiative heat fluxes $q_{\text{w1}}/\sigma T_{\text{w1}}^4$ on the lower

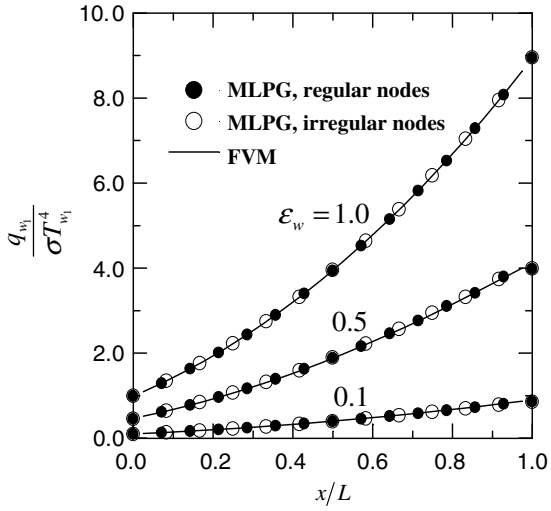

Fig. 8. Dimensionless net wall radiative heat flux in a gray enclosure with a purely scattering medium.

wall are presented in Fig. 8 in the case of $\omega = 1.0$ for three values of wall emissivities, namely 0.1, 0.5 and 1.0, and compared to the results obtained from the FVM presented in Ref. [12]. The MLPG results agree with those of FVM very well. No observable difference could be detected between the results of MLPG and FVM when they are presented in graphical form. The effects of the nodal irregularity are very small. Because of asymmetric distribution of refractive index, differing from the case of uniform refractive index, the profiles of dimensionless net radiative heat flux are asymmetric.

4. Conclusions

Because ray goes along a curved path determined by the Fermat principle, curved ray tracing is very difficult and complex in graded index medium. To avoid the difficult and complex computation of curved ray trajectories, the methods, which are not based on curved ray-tracing, need to be developed for the solution of radiative heat transfer in graded index medium. The discrete-ordinate equation of radiative transfer in three-dimensional semitransparent graded index media is presented. Then, a meshless local Petrov–Galerkin approach based on discrete-ordinate equations is developed to solve the radiative transfer problem in multi-dimensional absorbing–emitting–scattering semitransparent graded index media, in which a moving least square approximation is used to construct the shape function. Two particular test problems in radiative transfer are taken as examples to verify this meshless approach. The predicted temperature distributions and the dimensionless radiative heat fluxes are determined by the proposed method and compared with the other benchmark approximate solutions. The results show that the meshless local Petrov–Galerkin approach based on discrete-ordinate equations has a good accuracy in solving the radiative transfer problems in absorbing–emitting–scattering semitransparent graded index media.

Acknowledgement

The support of this work by the National Nature Science Foundation of China (50336010) is gratefully acknowledged.

References

[1] M. Born, E. Wolf, Principles of Optics, Cambridge University Press, New York, 1999.
[2] Y.T. Qiao, Graded Index Optics, Science Press, Beijing, 1991.
[3] P. Ben Abdallah, V. Le Dez, Temperature field inside an absorbing–emitting semitransparent slab at radiative equilibrium with variable spatial refractive index, J. Quantit. Spectros. Radiat. Transfer 65 (4) (2000) 595–608.
[4] P. Ben Abdallah, V. Le Dez, Thermal emission of a two-dimensional rectangular cavity with spatial affine refractive index, J. Quantit. Spectros. Radiat. Transfer 66 (6) (2000) 555–569.
[5] P. Ben Abdallah, V. Le Dez, Thermal emission of a semitransparent slab with variable spatial refractive index, J. Quantit. Spectros. Radiat. Transfer 67 (3) (2000) 185–198.
[6] P. Ben Abdallah, A. Charette, V. Le Dez, Influence of a spatial variation of the thermo-optical constants on the radiative transfer inside an absorbing–emitting semitransparent sphere, J. Quantit. Spectros. Radiat. Transfer 70 (3) (2001) 341–365.
[7] Y. Huang, X.L. Xia, H.P. Tan, Radiative intensity solution and thermal emission analysis of a semitransparent medium layer with a sinusoidal refractive index, J. Quantit. Spectros. Radiat. Transfer 74 (2) (2002) 217–233.
[8] Y. Huang, X.L. Xia, H.P. Tan, Temperature field of radiative equilibrium in a semitransparent slab with a linear refractive index and gray walls, J. Quantit. Spectros. Radiat. Transfer 74 (2) (2002) 249–261.
[9] L.H. Liu, Discrete curved ray-tracing method for radiative transfer in an absorbing–emitting semitransparent slab with variable spatial refractive index, J. Quantit. Spectros. Radiat. Transfer 83 (2) (2004) 223–228.
[10] L.H. Liu, H.C. Zhang, H.P. Tan, Monte Carlo discrete curved ray-tracing method for radiative transfer in an absorbing–emitting semitransparent slab with variable spatial refractive index, J. Quantit. Spectros. Radiat. Transfer 84 (3) (2004) 357–362.
[11] D. Lemonnier, V. Le Dez, Discrete ordinates solution of radiative transfer across a slab with variable refractive

index, J. Quantit. Spectros. Radiat. Transfer 73 (2–5) (2002) 195–204.
[12] L.H. Liu, Finite volume method for radiation heat transfer in graded index medium, J. Thermophys. Heat Transfer 19 (4) (2005), in press.
[13] G.R. Liu, Mesh Free Methods, CRC Press, Boca Raton, FL, 2003.
[14] X. Zhang, Y. Liu, Meshless Methods, Tsinghua University Press, Beijing, 2004.
[15] S.N. Atluri, S.P. Shen, The Meshless Local Petrov–Galerkin (MLPG) Method, Tech Science Press, Encino, CA, 2002.
[16] S.N. Atluri, T. Zhu, A new meshless local Petrov–Galerkin (MLPG) approach in computational mechanics, Computat. Mech. 22 (2) (1998) 117–127.
[17] M.F. Modest, Radiative Heat Transfer, second ed., Academic Press, San Diego, CA, 2003.
[18] J.C. Chai, H.S. Lee, S.V. Patankar, Improved treatment of scattering using the discrete ordinates method, J. Heat Transfer 116 (1) (1994) 260–263.
[19] H.P. Tan, Y. Huang, X.L. Xia, Solution of radiative heat transfer in a semitransparent slab with an arbitrary refractive index distribution and diffuse gray boundaries, Int. J. Heat Mass Transfer 46 (11) (2003) 2005–2014.